Benchmark: Axisymmetric liquid droplets on viscoelastic substrates

Leonie Schmeller*[1] and Dirk Peschka‡[1]

[1]Weierstrass Institute for Applied Analysis and Stochastics, 10117 Berlin, Germany

May 2022
DOI: 10.5281/zenodo.6556859

Abstract

We report on the data from a numerical benchmark of a stationary axisymmetric droplet on viscoelastic Neo-Hookean substrates obtained using FEniCS [3]. Numerical results using our Lagrangian phase-field approach [4] are compared with results by Van Brummelen et al. [6] and by Aland & Mokbel [2].

1 Problem description

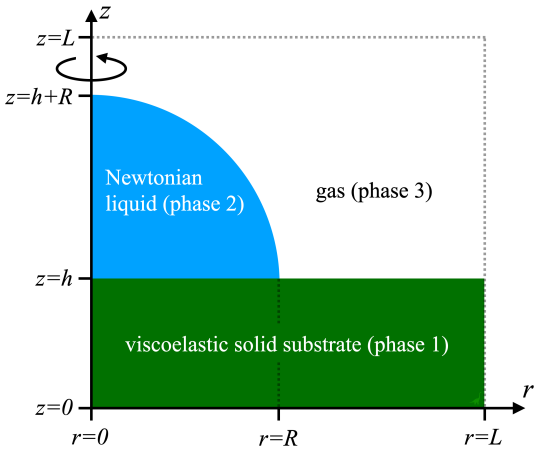

Figure 1: Sketch of axisymmetric droplet on viscoelastic substrate

*leonie.schmeller@wias-berlin.de
‡dirk.peschka@wias-berlin.de

We derived in [4] that the corresponding model of Neo-Hookean viscoelastic droplet relaxation can be written as a gradient flow, which we formulate in terms of a weak formulation, where we seek $q : [0,T] \to \mathscr{Q}$ such that

$$s(\partial_t q, v) = -\langle \mathrm{D}\mathscr{L}(q), v\rangle, \tag{1}$$

for all v from suitable spaces $\mathscr{Q}$. The state variable q contains displacements u and possible multiplier λ. The Lagrangian $\mathscr{L}$ defined in (2) is the sum of a free energy and possible incompressibility constraints using the deformation gradient $F = \mathbb{I} + \nabla u$. The bilinear form s is the Stokesian dissipation defined in (3). The liquid, solid and gas phase are encoded using *phase indicator* fields $\varphi_i : \Omega \to \mathbb{R}$ with $0 \le \varphi_i \le 1$ and $\sum_{i=1}^{3} \varphi_i(x) = 1$ for every $x \in \Omega$.

For this specific benchmark problem the phase indicators φ_i do not evolve in time, which for the continuous displacement field u corresponds to a no-slip boundary condition (continuous displacements and velocities) at the interface. The phase indicators are chosen so that the solid reference φ_1 has a flat interface at $z = h$ with the liquid and with the gas phase. The entire computational domain itself is

$$\Omega = \{(r,z) \in \mathbb{R}^2 : 0 < z, r < L\}.$$

Note that parts of the energy are written in terms of $-1 \le \psi_i = 2\varphi_i - 1 \le 1$. We use the spaces $u \in U = H^1_0(\Omega)$ and $\lambda \in \Lambda = L^2(\Omega)$ for displacement and multiplier, where the displacements vanish at $z = 0$ and $z = H$ and the horizontal component of the

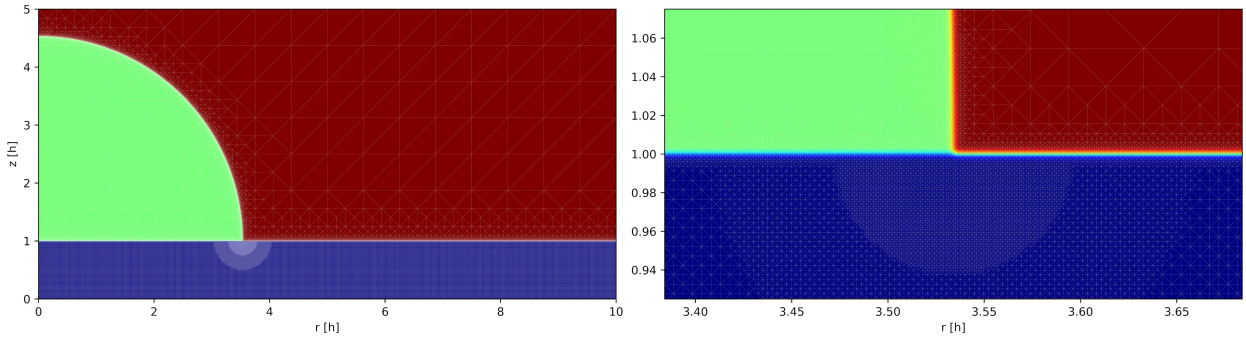

Figure 2: Locally refined undeformed mesh (white lines) of phase fields (color shading) at the interfaces showing substrate (blue), fluid (green) and gas (red).

displacements vanishes at $r = 0$ and $r = L$. The Lagrangian is has elastic, surface and compressibility contributions, where

$$\mathscr{L}(q) = \int_\Omega \big(E_{\text{elast}} + E_{\text{phase}} + E_{\text{comp}}\big)\,\mathrm{d}V \tag{2}$$

$$E_{\text{elast}} = \frac{G(\varphi_i)}{2}\operatorname{tr}(F^T F - \mathbb{I})$$

$$E_{\text{surf}} = \sum_{i=1}^{3} \frac{3\sigma_i}{2\sqrt{2}}\left[\frac{\varepsilon}{2}|F^{-T}\nabla\psi_i|^2 + \frac{1}{4\varepsilon}(\psi_i^2 - 1)^2\right]J$$

$$E_{\text{comp}} = \begin{cases} \lambda(J-1) & \text{incompressible} \\ \kappa(J-1)^2 & \text{compressible} \end{cases}$$

with volume element $\mathrm{d}V = 2\pi\, r\,\mathrm{d}r\,\mathrm{d}z$ and $J = \det F$. Note that for incompressible materials the second term in E_{surf} vanishes upon differentiation w.r.t u. For compressible solids the elastic energy E_{elast} contains a term $-\log(J)$, which we neglect since we are interested in the limit $\kappa \to \infty$. In the compressible case $q = u \in U = \mathscr{Q}$ with large penalization constant $\kappa \in \mathbb{R}$ and in the incompressible case $q = (u, \lambda) \in U \times \Lambda = \mathscr{Q}$ with Lagrange multiplier λ. The axisymmetric deformation gradient and scalar gradient that appear above are

$$\nabla u = \begin{pmatrix} \partial_r u_r & 0 & \partial_z u_r \\ 0 & \frac{1}{r}u_r & 0 \\ \partial_r u_z & 0 & \partial_z u_z \end{pmatrix}, \quad \nabla\psi = \begin{pmatrix} \partial_r\psi \\ 0 \\ \partial_z\psi \end{pmatrix}.$$

The elastic modulus is defined as the linear combination $G\big(\varphi_i\big)(x) = \sum_{i=1}^3 G_i\varphi_i(x)$ with constant $G_i \geq 0$.

For the viscous dissipation we use a (Lagrangian) Kelvin-Voigt Stokesian dissipation

$$s(w, v) = \int_\Omega \mu\nabla w : \nabla v\ \mathrm{d}V, \tag{3}$$

which is sufficient, since we are only interested in energy minimizers. We denote $A : B = \sum_{ij} A_{ij}B_{ij}$ the Frobenius inner product between matrices $A, B \in \mathbb{R}^{d\times d}$. In principle, one would have to use a Eulerian Kelvin-Voigt rheology with the viscosity $\mu = \mu(\varphi_i)$ and $\nabla w : \nabla v \to \operatorname{sym}(\nabla w F^{-1}) : \operatorname{sym}(\nabla v F^{-1})J$ with $\operatorname{sym} A = \frac{1}{2}(A + A^T)$ to be more realistic but should end up with the same energy minimizers (assuming uniqueness).

In the following we shortly elaborate on the used finite element space and time discretization. For this we are going to present result from an incompressible and a compressible model, where for the incompressible model we discretize the problem using P_1/P_1 elements for displacement and multiplier und for the compressible model we discretize the problem using P_2 elements to avoid locking phenomena common for nearly incompressible problems. After discretization in space we solve the fully implicit problem

$$s(q^n - q^{n-1}/\tau, v) = -\langle \mathrm{D}\mathscr{L}(q^n), v\rangle,$$

which guarantees descent of the free energy, see [4]. At the interfaces set by the indicator functions φ_i we perform local refinement of the mesh as shown in Fig. 2 to resolve the interface thickness $\varepsilon = 1/800$.

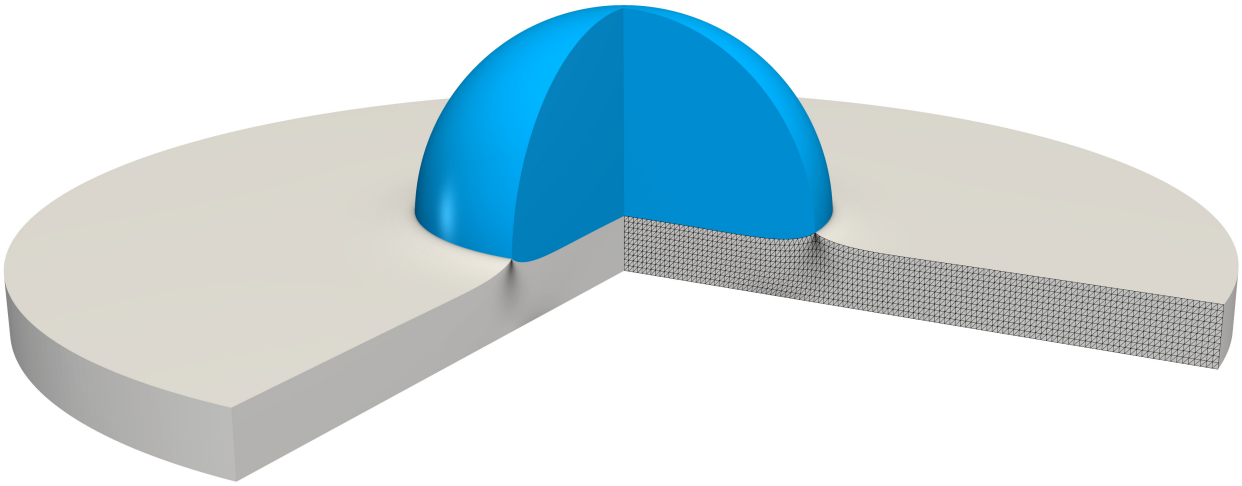

Figure 3: Stationary axisymmetric droplet (blue) on viscoelastic Neo-Hookean substrate (gray), where darker shading indicates larger energy density E_{elast}. Grid visualizes displacement of uniform planar substrate.

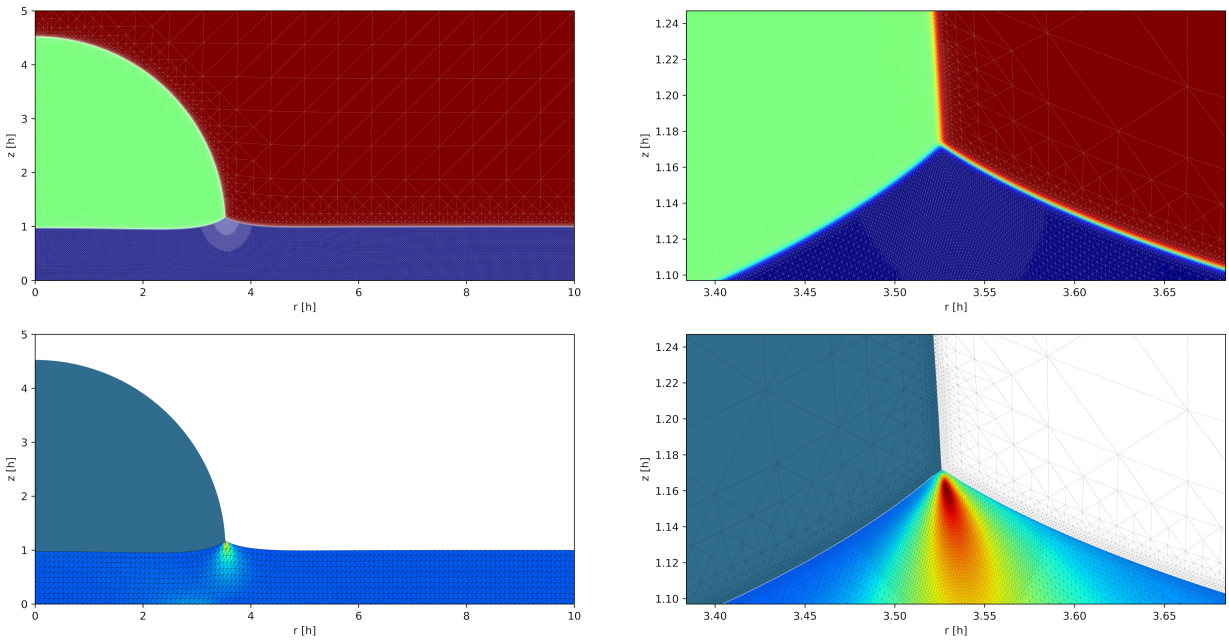

Figure 4: Stationary droplet for the axisymmetric domain $\Omega = [0, 10] \times [0, 10]$ showing (top left) phase fields combined into $\varphi = \sum_{i=1}^{3} i\varphi_i(x)$ and (botton left) elastic energy density E_{elast} in the solid substrate (blue=low, red=high) and (right column) corresponding quantities near the contact line. In lines in the lower left image highlight the displacement, while all other lines (black or white) show the mesh.

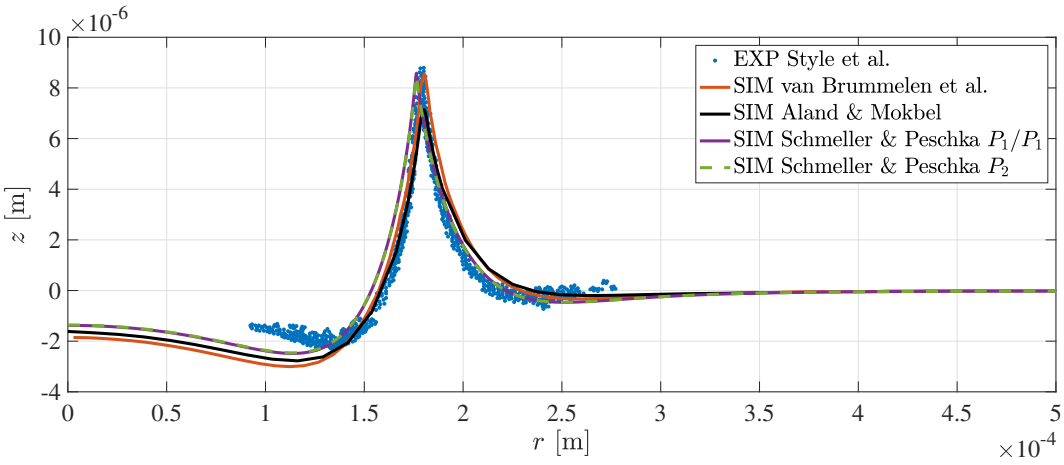

Figure 5: Benchmark comparison of experiments by Style et al. [5] in comparison with simulations by van Brummelen et al. [6] and Aland & Mokbel [1] compared to our simulations for incompressible materials with P_1/P_1 elements and compressible materials with P_2 elements and $\kappa = 10^4 G_1$.

2 Results

Following [6, 2] we choose the model parameters in Table 1 for the benchmark. Note the the surface tensions σ_i are related to the standard interfacial tensions via $\sigma_{\mathrm{sl}} = \sigma_1 + \sigma_2$ (solid-liquid), $\sigma_{\mathrm{sa}} = \sigma_1 + \sigma_3$ (solid-air), $\sigma_{\mathrm{la}} = \sigma_2 + \sigma_3$ (liquid-air) where

$$\sigma_{\mathrm{sl}} = 36 \cdot 10^{-3}\mathrm{Jm}^{-2},$$
$$\sigma_{\mathrm{sa}} = 31 \cdot 10^{-3}\mathrm{Jm}^{-2},$$
$$\sigma_{\mathrm{la}} = 46 \cdot 10^{-3}\mathrm{Jm}^{-2}.$$

The corresponding stationary solutions with P_1/P_1 FE are shown in Fig. 3 and Fig. 4. A direct comparison of the solid/liquid and solid/gas interface shape with the ones in [6, 2, 5] are shown in Fig. 5. For this benchmark comparison we provide the data summarized in Tab. 2. We provide a dataset for stationary solutions of the incompressible model with P_1/P_1 elements and for the compressible models with P_2 elements. Except for the `csv` files, each dataset comes with the computational mesh. The `pvd/vtu/xdmf` files were created in Python/FEniCS and imported and postprocessed with ParaView and FEniCS itself. The comparison of interface shapes stored in `csv` files were performed with MATLAB.

The overall agreement between the simulation appears good, taking into account the different numerical methods used, i.e.,

- phase fields vs sharp interfaces between the solid and the other two phases,
- Eulerian vs Lagrangian description of elasticity,
- the involved scaling limits $\varepsilon \to 0$ and vanishing Cahn-Hilliard mobility.

Acknowledgement

Both authors acknowledge the funding by the German Research Foundation (DFG) through the projects #422786086 (LS) and #422792530 (DP) within the DFG Priority Program SPP 2171 *Dynamic Wetting of Flexible, Adaptive, and Switchable Substrates*.

name	G_1	$G_{2,3}$	σ_1	σ_2	σ_3	L	R	ε
unit	Pa	Pa	$^{\mathrm{J}}/_{\mathrm{m}^2}$	$^{\mathrm{J}}/_{\mathrm{m}^2}$	$^{\mathrm{J}}/_{\mathrm{m}^2}$	h	h	h
value	10^3	0	$10.5 \cdot 10^{-3}$	$25.5 \cdot 10^{-3}$	$20.5 \cdot 10^{-3}$	10	$^{176.7}/_{50}$	$^{1}/_{800}$

Table 1: Benchmark parameters with lengths L, R, ϵ rescaled by substrate thickness $h = 5 \cdot 10^{-5}\,\mathrm{m}$

References

[1] S. Aland and D. Mokbel. Data Supplement for "A unified numerical model for wetting of soft substrates". *Zenodo*, 2020. doi: 10.5281/zenodo.4066988.

[2] S. Aland and D. Mokbel. A unified numerical model for wetting of soft substrates. *International Journal for Numerical Methods in Engineering*, 122(4):903–918, 2021.

[3] A. Logg, K.-A. Mardal, and G. Wells. *Automated solution of differential equations by the finite element method: The FEniCS book*, volume 84. Springer Science & Business Media, 2012.

[4] L. Schmeller and D. Peschka. Gradient flows for coupling order parameters and mechanics. *WIAS Preprint*, 2909:1–24, 2022. doi: 10.20347/WIAS.PREPRINT.2909.

[5] R. W. Style, R. Boltyanskiy, Y. Che, J. Wettlaufer, L. A. Wilen, and E. R. Dufresne. Universal deformation of soft substrates near a contact line and the direct measurement of solid surface stresses. *Physical Review Letters*, 110(6):066103, 2013.

[6] E. Van Brummelen, T. Demont, and G. van Zwieten. An adaptive isogeometric analysis approach to elasto-capillary fluid-solid interaction. *International Journal for Numerical Methods in Engineering*, 122(19):5331–5352, 2021.

filename	description
`stationary_P1P1.h5`	FEniCS readable HDF5 file: `postprocessing_P1P1.py` generates the `P1P1` files below
`P1P1_phi1.pvd`	incompressible P_1/P_1: φ_1 on deformed domain (plus vtu file)
`P1P1_phi2.pvd`	incompressible P_1/P_1: φ_2 on deformed domain (plus vtu file)
`P1P1_phi3.pvd`	incompressible P_1/P_1: φ_3 on deformed domain (plus vtu file)
`P1P1_u.pvd`	incompressible P_1/P_1: u on reference domain (plus vtu file)
`P1P1_mesh1.pvd`	incompressible P_1/P_1: deformed solid domain (plus vtu file)
`P1P1_mesh2.pvd`	incompressible P_1/P_1: deformed fluid domain (plus vtu file)
`P1P1_elastic.pvd`	incompressible P_1/P_1: elastic energy density on deformed domain (plus vtu file)
`P1P1_solution.xdmf`	incompressible P_1/P_1: elastic energy density, φ_i, u on reference domain (plus h5 file)
`P1P1_solution.png`	incompressible P_1/P_1: png image of solution
`stationary_P2.h5`	FEniCS readable HDF5 file: `postprocessing_P2.py` generates the `P2` files below
`P2_phi1.pvd`	compressible $P2$: φ_1 on deformed domain (plus vtu file)
`P2_phi2.pvd`	compressible $P2$: φ_2 on deformed domain (plus vtu file)
`P2_phi3.pvd`	compressible $P2$: φ_3 on deformed domain (plus vtu file)
`P2_u.pvd`	compressible $P2$: u on reference domain (plus vtu file)
`P2_mesh1.pvd`	compressible $P2$: deformed solid domain (plus vtu file)
`P2_mesh2.pvd`	compressible $P2$: deformed fluid domain (plus vtu file)
`P2_elastic.pvd`	compressible $P2$: elastic energy density on deformed domain (plus vtu file)
`P2_solution.xdmf`	compressible $P2$: elastic energy density, φ_i, u on reference domain (plus h5 file)
`P2_solution.png`	compressible $P2$: png image of solution
`benchmark.m`	MATLAB file reading `csv` data below & comparison with data from [1]
`P1P1_interface.csv`	interface shape data for incompressible simulation in `benchmark` folder
`P2_interface.csv`	interface shape data for compressible simulation in `benchmark` folder

Table 2: Description of data/files for the benchmark. The files `stationary_P1P1.h5` and `stationary_P2.h5` are readable in FEniCS using the `postprocessing_P1P1.py` and `postprocessing_P2.py` scripts. The `pvd/vtu/xdmf` files are readable with the ParaView visualization tool. The `csv` data tables are readable using the MATLAB script `benchmark.m`.